New Denoising Scheme for Magnetic Resonance Spectroscopy Signals

Osama A. Ahmed

Abstract—A new scheme for denoising magnetic resonance spectroscopy (MRS) signals is presented. This scheme is based on projecting noisy MRS signals in different domains, consecutively, and performing noise filtering operations in these domains. The domains are chosen such that the noise portion, which is inseparable from the desired signal in one domain, is separable in the other. A set of stable, linear, time-frequency (SLTF) transforms with different resolutions was selected for these projections as an example. Scheme evaluation was performed using extensive MRS signals with various noise levels. Compared with one domain denoising, it was observed that the proposed scheme gives superior results that compensate for the excess computational requirements. The proposed scheme supersedes also the wavelet packet denoising schemes.

Index Terms—Magnetic resonance spectroscopy, signal enhancement, time-frequency analysis, wavelet packet, wavelet transforms.

I. INTRODUCTION

MAGNETIC resonance spectroscopy is a potentially useful and effective diagnostic tool in basic research, clinical investigation, and disease diagnosis since it provides both chemical and physiological information about the tissue under investigation. Many MRS signals, however, are faced with several difficulties such as their very low signal-to-noise ratio (SNR) and their overlapping resonances with different transverse relaxation time (T_2) values. Signal averaging is used to increase the SNR, but this often results in a substantial increase in MRS acquisition time, which may not be tolerable in many situations, particularly for unstable biological compounds where long replications are not feasible. Conventional Fourier transform techniques improve the spectrum but they require long and tedious work by the spectroscopist [1]. Several noninteractive MRS denoising schemes have been developed [2]–[10]. MRS denoising is also important as a preprocessing step before parameter estimation for MRS automatic processing. Otherwise parameter estimation is difficult because of the model nonlinearity and the low SNR [8], [11].

Denoising in many applications is performed using a threshold function along with a transform such as Fourier, wavelet, or time-frequency transforms. The threshold function and the transform are preferred to be simple and easily calculated or implemented in integrated circuits. The transform is chosen according to its ability to represent the desired signal in a small number of coefficients which depends on the characteristics of both the signal and the transform. For instance, since MRS signals have time-dependant spectra (i.e., nonstationary signals), their Fourier transform spreads along the frequency axis and, thus, hinders the utilization of this transform to denoise MRS signals. On the contrary, time-frequency and time-scale transforms are adapted to nonstationary signals and many of them, such as Wigner distribution [12], Generalized Gabor transform [8], Zak transform [13], SLTF transform [9], and wavelet transforms [4]–[7], represent MRS signals in a small number of coefficients and hence provide better denoising capabilities.

Regardless the transform type, the following scheme is generally used: 1) transform the noisy signal into the new domain; 2) retain only the coefficients whose magnitudes are above a certain threshold which is usually related to the known or estimated noise standard deviation; and 3) perform the synthesis transform on the retained coefficients to get the noise-reduced signal. This scheme was named hard thresholding. Other thresholding techniques such as soft thresholding [14], [15], related thresholding [16]–[18], and global thresholding [19] have also been examined.

The retained signal, however, still has some noise which cannot be separated from the desired signal in this domain. The new scheme being proposed is to reproject the retained signal into another domain which is chosen such that the desired signal, in this domain, is still compact and is separable from the remaining noise (or part of it). Thus, performing an additional denoising process in the new domain may enhance the signal further.

A set of SLTF transforms with different time and frequency resolutions was selected in this paper as SLTF transform shows good MRS denoising results with minimal MRS signal distortion [9]. The proposed scheme, however, is applicable to other sets.

SLTF transform is specified by its number of analysis samples in frequency (N) which controls the time and frequency resolutions. Each choice of N leads to a different transform with different characteristics (denoted as SLTF_N). As will be shown in Section II, the compactness of MRS signal components (and hence the thresholding process) varies with N. The noisy MRS signal is project (and hence denoised) into various SLTF_N transforms with different N consecutively.

Denoising using the widely used wavelet packet and matching pursuit has close relation with the proposed scheme. Entropy-based wavelet packet [20], [21] and matching pursuit [22] are better generalization of the famous wavelet and filter bank. Wavelet packet and matching pursuit iteratively try to find the "best" representation of a signal with a relatively small

number of coefficients. The resulting representation can then be used more effectively for denoising at once. Wavelet packet denoising techniques have been applied to medical signals [23], [24]. The proposed scheme is different from these algorithms in the sense that the iterations are done on the denoised signal and not on the noisy residuals. Performance comparisons between the two schemes on MRS signals will be presented in the result section.

The paper is organized as follows. In Section II, the SLTF_N domain representation of MRS noise and one type of the MRS signal, namely free induction decay (FID), is discussed. The proposed scheme is illustrated in Section III. Some results and discussions on MRS signals are given in Section IV followed by concluding remarks in Section V. Details of the SLTF_N transform are given in the Appendix.

II. MRS-FID SIGNALS IN THE SLTF_N DOMAIN

Any MRS-FID signal, $x(k)$, can be modeled as a sum of Q exponentially damped complex exponents plus noise [25], i.e.,

$$x(k) = \sum_{q=1}^{Q} b_q \exp\left(-\frac{t_k}{T_{2q}} + j2\pi f_q t_k + j\phi_q\right) + z(k) \quad (1)$$

for $k = 0, \ldots, K-1$ where K is the signal length and b_q, f_q, ϕ_q, and T_{2q} are the amplitude, frequency, phase and relaxation time of the qth component, respectively, and $t_k = \Delta_t k$ with Δ_t being the sampling period. The noise term, $z(k)$, is well approximated by a complex white Gaussian noise with zero mean and standard deviation σ [26].

Each MRS component, $b_q \exp(-(t_k/T_{2q}) + j2\pi f_q t_k + j\phi_q)$, is represented in the SLTF_N domain (see Appendix) by a spike centered at f_q on the frequency axis and decays exponentially along the time direction [9]. The spike compactness in the SLTF_N domain depends on many factors. One of them is the ratio between the MRS component relaxation time, T_{2q}, and the number of analysis samples in frequency (N). To show this dependency, let

$$x_1(k) = 32 \exp\left(-\frac{t_k}{3} + j3000\pi t_k + 55°\right)$$

be a one-component noise-free MRS signal of length 1024. Fig. 1(a) and (b) represents intensity plots of x_1 in the SLTF_{32} and SLTF_{256} domains, respectively. The number of coefficients whose energy is greater than 1% of the total energy is 13 and 62 for SLTF_{32} and SLTF_{256} domains, respectively. Clearly, x_1 has more compact representation in the SLTF_{32} domain than in the SLTF_{256} domain. Alternatively, let

$$x_2(k) = 32 \exp\left(-\frac{t_k}{60} + j3000\pi t_k + 55°\right)$$

be a noise-free one-component MRS signal that differ from $x_1(k)$ only in the T_{2q} values. In Fig. 2, x_2 is plotted in the SLTF_{32} and SLTF_{256} domains. The number of coefficients whose energy is greater than 1% of the total energy is 182 and 46 for SLTF_{32} and SLTF_{256} domains, respectively. x_2 is more compact in the SLTF_{256} domain than in the SLTF_{32} domain.
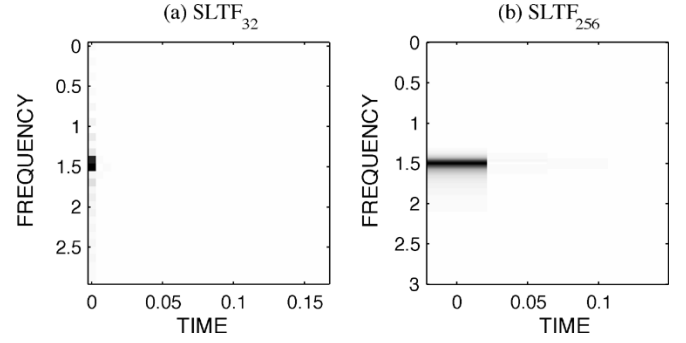
Fig. 1. $x_1(k)$ in two different SLTF domains.
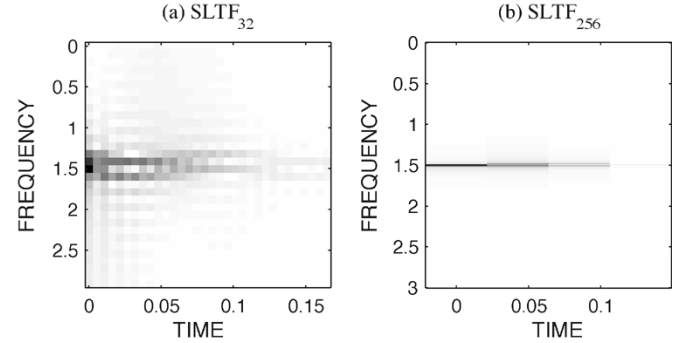
Fig. 2. $x_2(k)$ in two different SLTF domains.

The above examples show how the compactness of MRS components in the SLTF_N domain varies with N with respect to T_{2q}. MRS signals, however, are generally composed of different components with different T_{2q} values. Thus, for one SLTF_N transform with a particular N, some components are more compact than others. This situation may be reversed for different choice of N.

On the other hand, the MRS noise is evenly distributed among SLTF_N coefficients regardless of the choice of N as seen in Fig. 3 where a real life MRS noise, taken from VARIAN MERCURY-300, is plotted in the SLTF_{32} and in the SLTF_{256} domains. Clearly, for both cases, the noise is fairly distributed in the entire time-frequency domain. This is theoretically expected since MRS noise is well approximated by an additive white Gaussian process and since SLTF_N transform is a linear, near-orthogonal transform [27].

III. THE DENOISING SCHEME

The SLTF_N coefficients of the noisy MRS signals are of two types: one is dominated by noise and the other is dominated by the desired signal that has higher amplitude than the former. Denoising the MRS signal is achieved by filtering out the noise-dominated coefficients using any thresholding technique. An example would be the use of hard thresholding technique where all transform coefficients whose energies are lower than a certain threshold are set to zero.

The success of this denoising method depends on the difference between the amplitude of the two types. This depends on the transform's ability to represent MRS signals in a small number of coefficients. For example, if the number of the two types is equal, approximately 50% of the noise will be removed
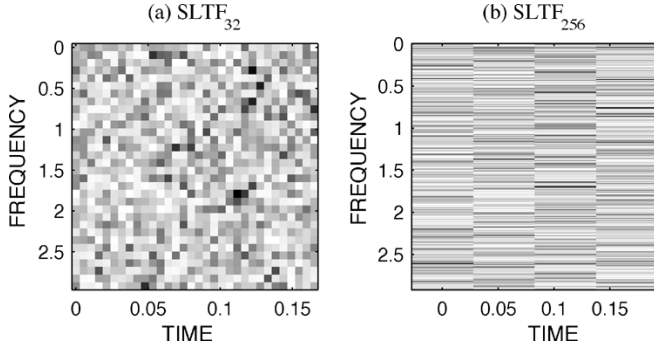
Fig. 3.   Real NMR noise in the SLTF domain.

by filtering. The retained coefficients, however, still contain approximately 50% of the noise in addition to the desired signal.

Projecting the signal again into another SLTF_N domain with a different N will redistribute both the signal and the residual noise in such a way that some MRS components will be more compact (i.e., the energy of this MRS component will be contained in fewer coefficients while the neighboring coefficients will have less energy which will be removed by filtering); the other MRS components will be less compact (i.e., the neighboring coefficients will have more energy and will not be affected by filtering providing that the threshold value is chosen to be sufficiently low to pass these coefficients). Thus, further signal enhancement can be achieved by filtering out the noise-dominated coefficients in the new domain.

The threshold value (t) is usually chosen to be proportional to the noise standard deviation (σ), i.e., $t = c\sigma$ where c is a constant. Choosing the proportionality constant c has been treated in many papers such as [15], [28]–[30]. For example, in [29] $c \in (3, 4)$ was chosen based on the fact that most of the noise values will fall within 3–4 times of its standard deviation. In [15], c was chosen as $\sqrt{2 \log K}$.

In this paper, a fixed threshold value is taken for all transforms providing that SLTF transforms possess the energy preservation property. The threshold value is chosen to be sufficiently less than the optimal value $t < \sigma\sqrt{2 \log K}$ to ensure that in the worst case where one MRS component looses its compactness during any transformation, minimal part of this component is filtered out. Assuming that the recording time is sufficiently large, σ can be estimated in advance by calculating the power of the last data points which are entirely noise.

The steps of the proposed scheme are as follows.

1) Estimate the noise variance σ using the last data points.
2) Take $t = g\sigma\sqrt{2 \log K}$ where $0 < g < 1$.
3) Select a set $(\mathbf{N})$ containing r suitable values of N: $\mathbf{N} = \{N_1, N_2, \ldots, N_r\}$.
4) For $i = 1, r$:
    - compute SLTF_{N_i} transform of the noisy MRS signal;
    - retain only the coefficients whose magnitudes are greater than t;
    - compute the inverse SLTF_{N_i} transform on the retained coefficients to obtain a noise-reduced signal.

To test the denoising performance of the proposed scheme, the visual spectrum in addition to the SNR will be used in the

TABLE I
PARAMETERS OF SIMULATED PHOSPHORUS FID

Peak	fq (Hz)	dq (ms)	bq	ϕq (°)
Reference	-1590	11	32,000	55
P_i	-600	2	10,000	83
PCr	-60	20	6,000	98.5
γ	240	6	9,000	107.5
α	860	3	8,000	122.5
β	1900	5	4,000	153
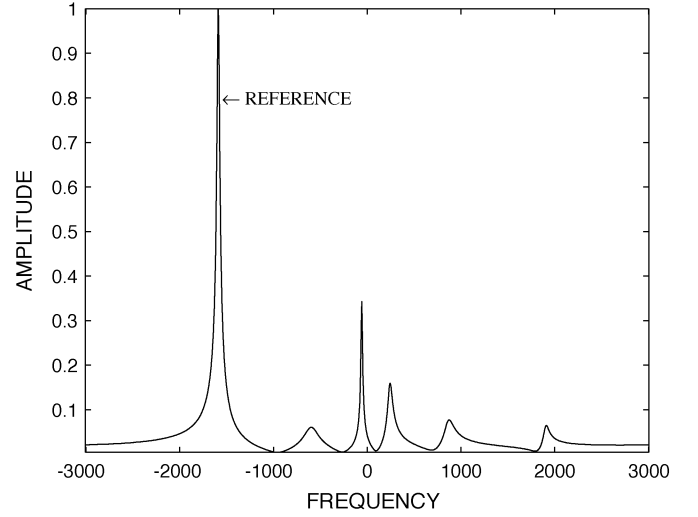
Fig. 4.   Spectrum of the phosphorus FID without noise.

next section. Since MRS signals are time varying, the SNR is defined as the signal energy over the energy of the noise in the observation period in decibels. MRS spectroscopist, however, may be interested in measuring the noise in the areas under each peak. Therefore, the following measure will be also used to test the denoising performance: calculate the SNR only in a 100 Hz window around each peak of the spectrum (denoted as $\overline{\mathrm{SNR}}$).

IV. RESULTS

Several simulations were performed on synthesized representative MRS signals with different SNR values. The results showed superior denoising performance for the proposed scheme that compensates the extra required calculations. As an example, the simulated phosphorus FID signal (distorted to explore a wider range of the parameter values) was chosen to closely match the real data [12], [13]. This signal (S) is 1024 points with a sampling period $\Delta_t = 166.2 \ \mu$s. The signal S is composed of six peaks. The frequencies, damping factors, amplitudes, and phases are given in Table I and the spectrum is shown in Fig. 4.

A zero-mean complex Gaussian noise, Z, is added to the signal where $\sigma = 2500$. Hence, The SNR is equal to $10 \log(\|S\|/\|Z\|) = 5.0$ dB. The corresponding spectrum, Fig. 5, shows that the noise hides the P_i, γ, α, and β components completely.

To denoise these signal using the proposed scheme, the values $\mathbf{N} = \{16, 32, 64\}$ and $g = 0.55$ are selected. The spectrum of the resulting denoised signal (S_1) is shown in Fig. 6. The
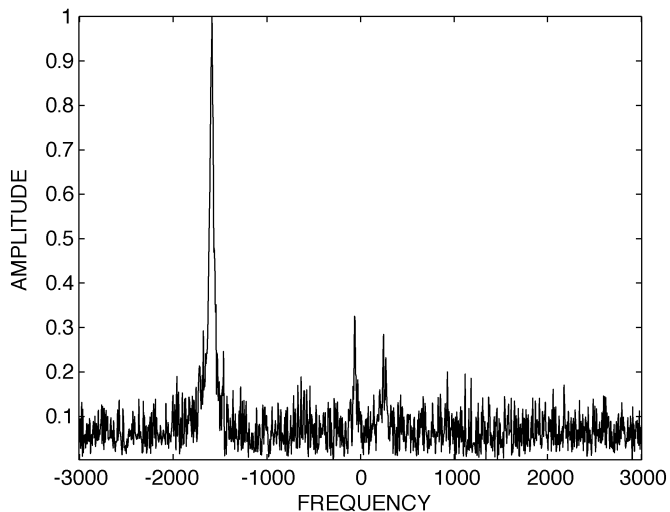
Fig. 5.   Spectrum of the noisy phosphorus FID.
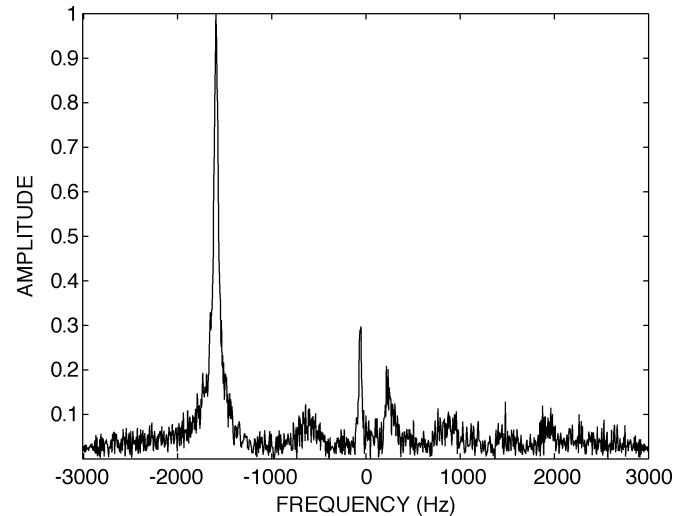
Fig. 7.   Enhanced spectrum using SLTF_{64}.
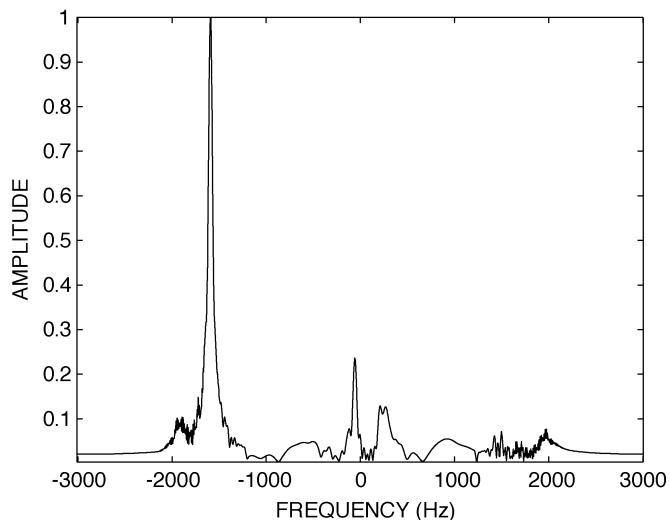
Fig. 6.   Enhanced spectrum using the new scheme.

Fig. 8.   Enhanced spectrum using wavelet-packet.

six peaks are identifiable in the spectrum of S_1. The SNR after processing is

$$\mathrm{SNR}_{\mathrm{after}} = 10 \log \left(\frac{\|S\|}{\|S_1 - S\|} \right) = 15.35 \text{ dB}$$

i.e., the SNR gain is 10.35 dB. For comparison, denoising the same signal using hard thresholding in the SLTF_{16}, SLTF_{32}, SLTF_{64} domains (each one alone as in [9]) gave $\mathrm{SNR}_{\mathrm{after}} = 10.19, 8.78, 10.53$ dB, respectively. The spectrum of the enhanced signal using SLTF_{64} (the best among the three) is shown in Fig. 7.

Denoising using wavelet packet analysis is a related widely used scheme which iteratively tries to find the "best" representation of a signal through its adequate display with a relatively small number of coefficients before denoising. To compare the proposed scheme with wavelet packet denoising scheme, a wavelet packet library composed of symlet wavelets of order 5 was used [31]. The wavelet packet decomposition is performed up to the 5th level and the optimal decomposition is determined

according to the entropy-based threshold $\sigma \sqrt{2 \log K}$. The denoised signal has $\mathrm{SNR} = 10.1$ dB and its spectrum is shown in Fig. 8.

Increasing the decomposition levels to 8 did not enhance the spectrum or the SNR value. Using another wavelet packet library of Daubechies wavelets [31] of order 3 with the same condition, gives $\mathrm{SNR} = 9.92$ dB. For $\overline{\mathrm{SNR}}$ measure: $\overline{\mathrm{SNR}}$ before processing was 13.8 dB. After processing, $\overline{\mathrm{SNR}}$ increased to 14.7 dB, 15.1 dB, 20.7 dB for Daubechies wavelet packet, symlet wavelet packet, and the proposed scheme, respectively.

Secondly, various MRS noises with different noise power were added to the same 1024-point phosphorus FID signal. The noisy signals were cleaned up using the following.

1) Single SLTF_{64} transform.
2) Wavelet packet with a library of:
    a) Coiflet Wavelets of order 1 (Coif1);
    b) Daubechies wavelets of order 3 (db3);
    c) symlet wavelet of order 5 (sym5).
3) The proposed scheme with $\mathbf{N} = \{16, 32, 64\}$ and $g = 0.55$.

TABLE II
SNR ENHANCEMENT

SNR_{before}			SNR_{after} using		
	$SLTF_{64}$	$Coif1$	$sym5$	$db3$	Proposed
9.40	12.9	14.3	14.2	14.9	19.1
6.90	10.3	11.7	11.6	12.0	16.7
4.92	8.49	8.98	9.77	9.69	15.3
3.30	7.09	7.45	8.32	8.08	13.9
2.00	5.74	5.52	6.47	6.40	13.1

TABLE III
$\overline{SNR}$ ENHANCEMENT

$\overline{SNR}_{before}$			$\overline{SNR}_{after}$ using		
	$SLTF_{64}$	$Coif1$	$sym5$	$db3$	Proposed
18.5	21.4	19.0	19.1	19.7	23.8
15.9	18.8	16.8	16.6	17.1	21.4
13.9	16.8	14.5	14.6	14.9	19.1
12.3	15.8	12.9	13.2	12.9	17.9
10.9	14.31	11.3	11.9	11.4	17.3

TABLE IV
THE NUMBER OF CONSECUTIVE PROJECTIONS (r) EFFECT

r	N	SNR	Gain	$\overline{SNR}$	Gain
1	{16}	9.59	2.40	18.35	2.10
2	{16, 32}	12.27	2.68	20.31	1.96
3	{16, 32, 64}	15.31	3.04	21.73	1.42
4	{16, 32, 64, 128}	16.92	1.61	21.80	0.08
5	{16, 32, 64, 128, 256}	16.88	-0.04	21.49	-0.32

TABLE V
SNR AND $\overline{SNR}$ ENHANCEMENTS FOR DIFFERENT (N)

N	SNR	$\overline{SNR}$
{16, 32, 64, 128}	16.92	21.80
{128, 64, 32, 16}	16.91	21.82
{8, 16, 32, 64}	16.40	21.07
{32, 64, 128, 256}	16.08	22.13

The average of the results of 10 runs for each value is shown in Table II for SNR and Table III for $\overline{SNR}$. The proposed scheme has remarkable better results for all SNR values than the others.

To study the effect of the r value (the number of projections) on the denoising performance, the phosphorus FID signal with $SNR_{before} = 7$ dB was denoised using the proposed scheme with $g = 0.45$ and different values of $r = 1, 2, 3, 4, 5$. The average of the results of 10 runs of SNR and $\overline{SNR}$ after processing are shown in Table IV along with the gain of introducing another projection (i.e., $Gain = SNR|_r - SNR|_{r-1}$). Apparently, the gain decreases with increasing r. Choosing $r \geq 4$ may not compensate for the required extra calculations.

Also, to study the effect of the choice of the r elements of N on the denoising performance, the above signal was denoised using four consecutive $SLTF_N$ transforms with different N as shown in Table V. First and second rows show less significance for the order of the values of N. The r elements of N, however, should be chosen carefully. It was found from this experiment, and others, that choosing N to be as close as possible to M (or $N \approx M \approx \sqrt{K}$) always gives the best results. For example, for $K = 1024$, choosing N around 32 (i.e., for $r = 3$, N = {16, 32, 64} gives the best result).

In another experiment, a signal is derived from an *in vivo* ^{31}P spectrum measured in the human brain and consists of 11 peaks [32]. The brain tissue ^{31}P peaks contain phosphomonoesters, inorganic phosphate, phosphodiesters, phosphocreatine, adeno-
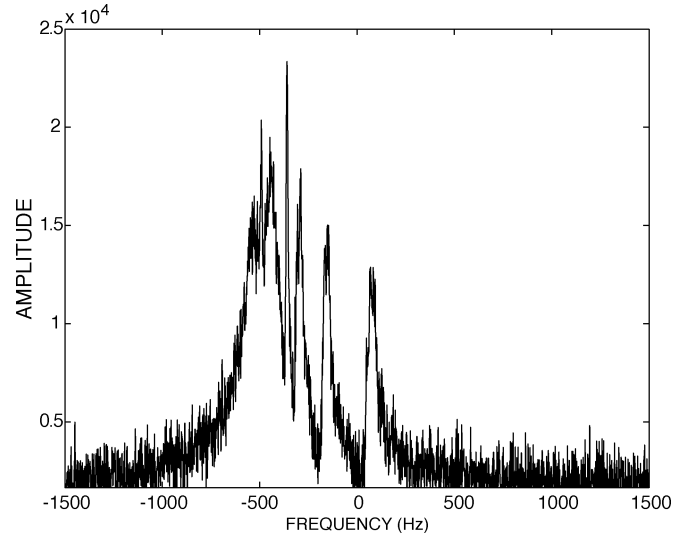
Fig. 9. *In vivo* ^{31}P spectrum measured in the human brain.
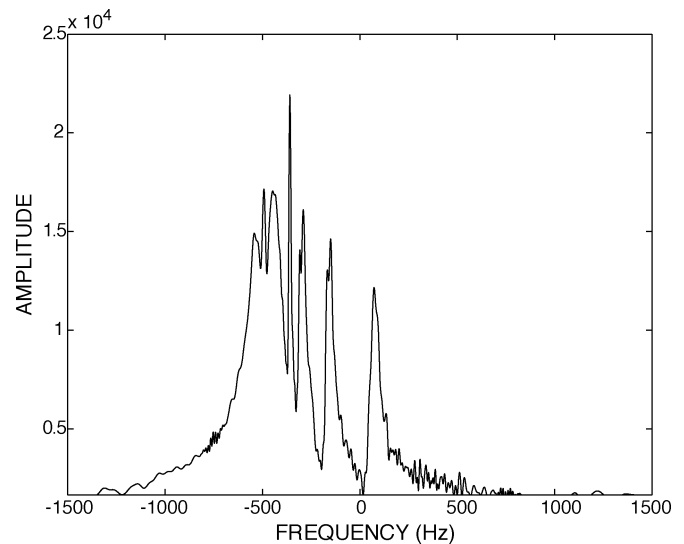
Fig. 10. Denoised human brain *in vivo* ^{31}P spectrum with the proposed scheme.

sine triphosphate: α-ATP, β-ATP, and γ-ATP. The time sampling interval is 0.333 ms. After adding MRS noise, the SNR is approximately 12.1 dB; Fig. 9. This signal was cleaned up using the proposed scheme with $g = 0.48$ and N = {8, 16, 32}. After processing, Fig. 10, the SNR increased to 23 dB. For comparison, denoising the same signal using the same thresholding technique but in one domain only gave SNR = 15, 14.8, 15.1, 15.1 dB for $SLTF_{64}$, $SLTF_{32}$, $SLTF_{16}$, $SLTF_8$, respectively. Denoising the same signal using wavelet packet gave SNR = 15.4, 17.3, 14.9 dB for Coiflet Wavelet of order 1, Daubechies wavelets of order 2, symlet wavelet of order 5 library, respectively. The denoised spectrum of Daubechies wavelet packet is shown in Fig. 11.

Finally, the same human brain *in vivo* ^{31}P signal, with high noise, was denoised using the proposed scheme with $g = 0.48$ and N = {8, 16, 32}. The SNR was approximately 4.9 dB before processing, Fig. 12, which increased to 17.7 dB after pro-
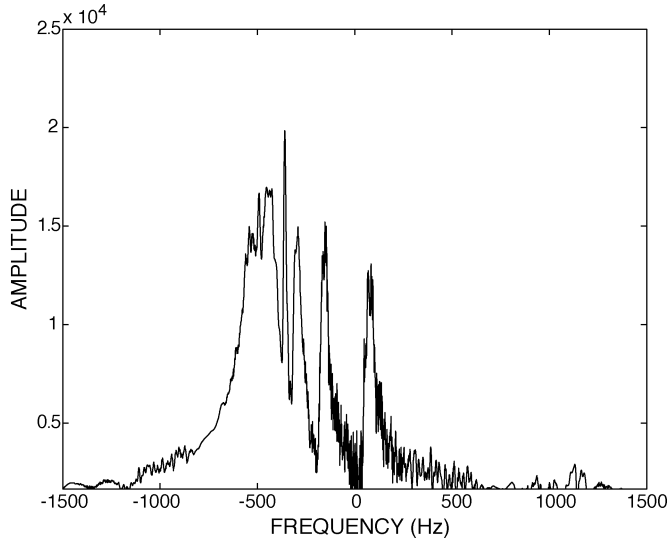
Fig. 11.   Denoised human brain *in vivo* ^{31}P spectrum with wavelet packet.
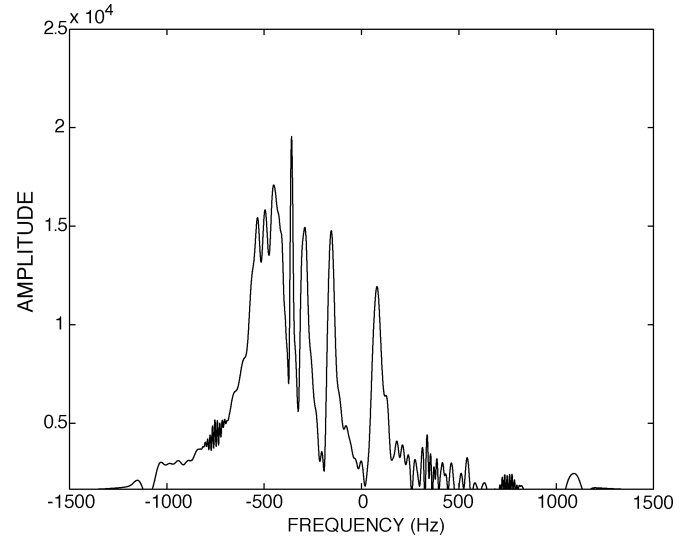
Fig. 13.   Denoised low SNR human brain ^{31}P spectrum.
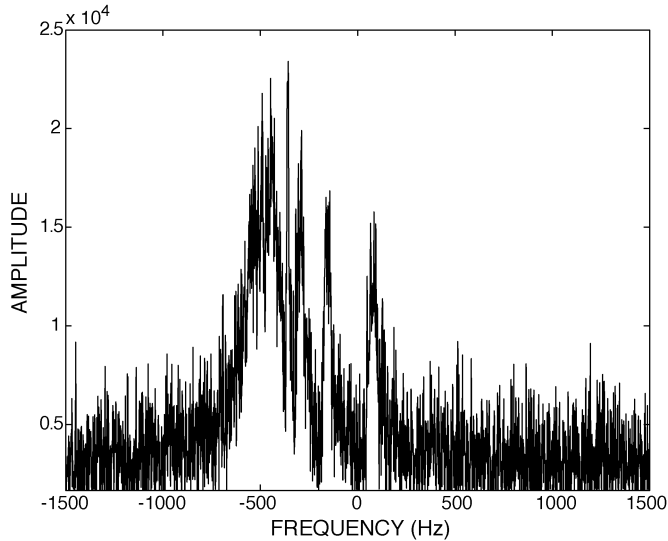
Fig. 12.   Low SNR human brain *in vivo* ^{31}P spectrum.

cessing, Fig. 13. Denoising the same signal using Daubechies wavelet packet gave $\mathrm{SNR} = 11.4$ dB.

V. Conclusion

A new scheme has been introduced for denoising MRS signals. This scheme is based on projecting the noisy MRS signal on several SLTF domains, consecutively, and performing hard thresholding on all of them according to the noise power. A set of SLTF transforms with different resolutions was selected. The proposed scheme surpasses the usual one domain denoising at the expense of increasing the computation time. Thus, the proposed scheme may be useful in situations where SNR is low. A comparison with the wavelet packet was performed based on visual spectrum, SNR, and a new measure. The proposed scheme produced superior results.
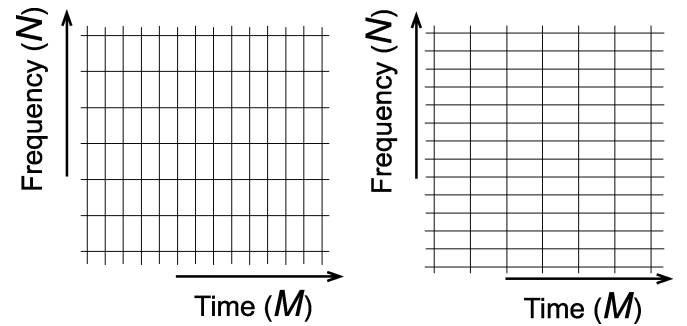
Fig. 14.   Tiling of the time-frequency plane for different choices of N.

Appendix
SLTF$_N$ Transform

The SLTF_N is a stable, linear, critically sampled, time-frequency transform [27]. The discrete SLTF is defined for a for a finite extent $(0 \leqslant k \leqslant K)$ discrete signal $x(k)$ as

$$a_{m,n} = \sum_{k=0}^{K-1} x(k)\gamma_m^*(k)\mathrm{csin}(k,n)_N$$

$$x(k) = \sum_{m=0}^{M-1}\sum_{n=0}^{N-1} a_{m,n}h(k-mN)\mathrm{csin}\frac{\pi\left(k+\frac{1}{2}\right)\left(n+\frac{1}{2}\right)}{N} \quad (2)$$

for $m = 0, \ldots, M-1$ and $n = 0, \ldots, N-1$ where $a_{m,n}$ are the transform coefficients, $\mathrm{csin}(.)$ stands for $\cos(.)$ for even m and $\sin(.)$ for odd m, $h(k)$ is the discrete Gaussian window function

$$h(k) \triangleq \exp\left(-\frac{\pi}{2N^2}\left(k-\frac{N-1}{2}\right)^2\right)$$

where $\gamma(k)$ is the biorthogonal function to $h(k)$ [27]. M and N are the number of analysis samples in time and frequency, respectively. This transform is critically sampled which means that the number of coefficients $MN = K$. N controls the frequency and time resolution in the time-frequency domain as shown in Fig. 14 where every cell represents a single time-frequency atom. Short-time atoms (the left tiling) are suitable for
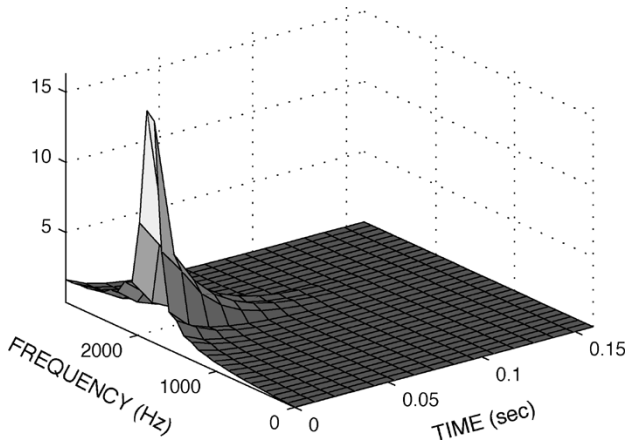
Fig. 15.   Modulated exponent in SLTF domain.

signals that have fast varying characteristics but have low frequency resolution. On the other hand, long-time atoms (the right tiling) are good for signals that have slowly varying characteristics. Frequency spreading may occur when long-time atoms are used for fast varying signals and vice versa. Thus, each choice of N produces one SLTF transform (SLTF_N) that is more suitable for certain signal type.

Compared with other time-frequency transforms, SLTF has several advantages, such as, it is a linear transform that makes the synthesis transform quite easy to compute. This is in contrast to bilinear (quadratic) distributions (such as the Wigner distribution [12]) where difficulties are encountered in retrieving the signal from the time-frequency domain. In addition, there is no cross-term interference that is produced in the bilinear distributions.

Moreover, SLTF is a critically sampled transform, which means that the transform coefficients are independent. Consequently, performing the synthesis transform after filtering is only a matter of matrix multiplication. This is in contrast to the over-sampled transforms where iterative methods are needed for the synthesis transform [33].

Compared with other critically sampled time-frequency transforms, such as the Generalized Gabor Transform used in [8] to enhance MRS signals, SLTF has two major advantages: excellent localization of the biorthogonal function and good numerical stability [9].

In addition, a fast algorithm to calculate the SLTF synthesis and analysis transforms, for $N = 2^q$ where q is integer, is presented in [34]. Using the fast algorithm, it requires only $K(\log_2 K - (1/2) \log_2 N)$ multiplications and $K(2 \log_2 K - \log_2 N - 3)$ additions for both the analysis and the synthesis transform computations and $K(2 \log_2 M + 5)$ multiplications and $K(4 \log_2 M - (3/2))$ additions for the biorthogonal function calculations.

For MRS signals, the SLTF coefficients of the MRS component $x_q(k) = b_q \exp(-(t_k/T_{2q}) + j2\pi f_q t_k + j\phi_q)$ are

$$a_{m,n} = b_q \sum_{k=0}^{K-1} \gamma_m^*(k) \operatorname{csin} \frac{\pi \left(k - \frac{1}{2}\right)\left(n + \frac{1}{2}\right)}{N}$$

$$\cdot \exp\left(-\frac{\Delta_t k}{T_{2_q}} + j2\pi f t_k + j\phi_q\right). \quad (3)$$

The magnitude of $a_{m,n}$ are plotted in Fig. 15 for Δ_t, b_q, T_{2q}, f_q, ϕ_q being 166.2 μs, 32, 22 ms, 1880 Hz, 55°, respectively. From Fig. 15, $x_1(k)$ is represented in the SLTF domain by a spike centered at f in the frequency direction and decays along the time direction.

REFERENCES

[1] J. C. Lindon and A. G. Ferrige, "Digitization and data processing in Fourier transform NMR," *Progress NMR Spectroscopy*, vol. 14, no. 1, pp. 27–66, 1980.

[2] Y. Lin and L. Hwang, "NMR signal enhancement based on matrix property mappings," *J. Magn. Reson. Ser. A*, vol. 103, pp. 109–114, 1993.

[3] H. Itagaki, "Improvements of nuclear magnetic resonance image quality using iterations of adaptive nonlinear filtering," *IEEE Trans. Image Process.*, vol. 12, no. 2, pp. 322–328, Jun. 1993.

[4] M. E. Alexander, R. Baumgarter, A. Summers, C. Windishberger, M. Klarhoefer, E. Moser, and R. Somorjai, "A wavelet-based method for improving signal-to-noise ratio and contrast in MR images," *Magn. Reson. Imag.*, vol. 18, no. 2, pp. 169–180, 2000.

[5] R. Nowak, "Wavelet-based rician noise removal for magnetic resonance imaging," *IEEE Trans. Image Process.*, vol. 8, no. 3, pp. 1408–1419, Mar. 1999.

[6] S. Zaroubi and G. Goelman, "Complex denoising of MR data via wavelet analysis: application for functional MRI," *Magn. Reson. Imag.*, vol. 18, no. 1, pp. 59–68, 2000.

[7] X. Shao, H. Gu, J. Wu, and Y. Shi, "Resolution of the NMR spectrum using wavelet transform," *Appl. Spectroscopy*, vol. 543, pp. 731–738, 2000.

[8] Y. Lu, S. Joshi, and J. M. Morris, "Noise reduction for NMR FID signals via Gabor expansion," *IEEE Trans. Biomed. Eng.*, vol. 44, no. 6, pp. 512–528, Jun. 1997.

[9] O. Ahmed and M. Fahmy, "NMR signal enhancement via a new time-frequency transform," *IEEE Trans. Med. Imag.*, vol. 20, no. 10, pp. 1018–1025, Oct. 2001.

[10] J. Antoine and A. Coron, "Time-frequency and time-scale approach to magnetic resonance," *J. Computat. Methods Sci. Eng.*, vol. 1, pp. 327–352, 2001.

[11] H. Chen, S. Van Huffel, C. Decanniere, and P. Vanhecke, "A signal-enhancement algorithm for the quantification of NMR data in the time-domain," *J. Magn. Reson. Ser. A*, vol. 109, no. 1, pp. 46–55, 1994.

[12] J. Leclerc, "Time-frequency representation of damped sinusoids," *J. Magn. Reson.*, no. 95, pp. 10–31, 1991.

[13] P. Angelidis and G. Sergiads, "Time-frequency representation of damped sinusoids using the Zak transform," *J. Magn. Reson. Ser. A*, no. 103, pp. 191–195, 1993.

[14] J. Weaver, Y. Xu, D. Healy, and J. Driscoll, "Filtering MR images in the wavelet transform domain," *Magn. Reson. Med.*, vol. 21, pp. 288–295, 1991.

[15] D. Donoho, "De-noising by soft-thresholding," *IEEE Trans. Inf. Theory*, vol. 41, no. 4, pp. 613–627, Apr. 1995.

[16] B. Delyon and A. Juditsky, "On minimax wavelet estimators," *J. Appl. Computat. Harmonic Anal.*, vol. 3, pp. 215–228, 1996.

[17] K. Tribouley, "Practical estimation of multivariate densities using wavelet methods," *Statistica Neerlandica*, vol. 49, pp. 41–62, 1995.

[18] D. Donoho, I. Johnstone, G. Kerkyacharian, and D. Picard, "Density estimation by wavelet thresholding," *Ann. Statist.*, vol. 24, pp. 508–539, 1996.

[19] G. Kerkyacharian, D. Picard, and K. Tribouley, "Lp adaptive density estimation," *Bernoulli*, vol. 2, pp. 229–247, 1996.

[20] R. Coifman and M. Wickerhauser, "Entropy based algorithms for best basis selection," *IEEE Trans. Inf. Theory*, vol. 38, no. 3, pp. 713–718, Mar. 1992.

[21] N. Hess-Nielsen and M. V. Wickerhauser, "Wavelets and time-frequency analysis," *Proc. IEEE*, vol. 84, no. 4, pp. 523–541, Apr. 1996.

[22] S. Mallat and Z. Zhang, "Matching pursuits with time-frequency dictionaries," *IEEE Trans. Signal Process.*, vol. 41, no. 12, pp. 3397–3415, Dec. 1993.

[23] R. Coifman and M. Wickerhauser, "Experiments with adapted wavelet de-noising for medical signals and images," in *Time-Frequency and Wavelets in Biomedical Engineering*, M. Akay, Ed. Piscataway, NJ: IEEE Press, 1998, pp. 323–346.

[24] J. Wood and K. Johnson, "Wavelet packet denoising of magnetic resonance images: importance of rician noise at low snr," *Magn. Reson. Med.*, vol. 41, pp. 631–635, 1999.

[25] M. Joliot, B. M. Mazoyer, and R. H. Heusman, "*In vivo* NMR spectral parameter estimation: a comparison between time and frequency domain methods," *Magn. Reson. Med.*, vol. 18, pp. 358–370, 1991.

[26] A. Abragam, The Principles of Nuclear Magnetism, Oxford, U.K., 1961.

[27] O. Ahmed and M. Fahmy, "Stable critically sampled Gabor transform with localized biorthogonal function," in *Proc. IEEE Int. Symp. Time-Frequency and Time-Scale Analysis*, Pittsburgh, PA, Oct. 1998, pp. 37–40.

[28] B. Delyon and A. Juditsky, "On minimax wavelet estimators," *J. Appl. Computat. Harmonic Anal.*, vol. 3, pp. 215–228, 1996.

[29] Q. Pan, L. Zhang, G. Dai, and H. Zhang, "Two denoising methods by wavelet transform," *IEEE Trans. Signal Process.*, vol. 47, no. 12, pp. 3401–3406, Dec. 1999.

[30] L. Zhang, P. Bao, and Q. Pan, "Threshold analysis in wavelet-based denoising," *Electron. Lett.*, vol. 37, no. 24, pp. 1485–1486, Nov. 2001.

[31] I. Daubechies, *Ten Lectures on Wavelets*. Philadelphia, PA: SIAM, 1992.

[32] L. Vanhamme, A. van den Boogaart, and S. Van Huffel, "Improved method for accurate and efficient quantification of mrs data with use of prior knowledge," *J. Magn. Reson.*, no. 129, pp. 35–43, 1997.

[33] S. Qian and D. Chen, *Joint Time-Frequency Analysis: Methods and Applications*. Upper Saddle River, NJ: Prentice-Hall PTR, 1996.

[34] O. Ahmed, "Fast computation of discrete SLTF transform," in *Proc. 11th IEEE Workshop Statistical Signal Processing*, Singapore, Aug. 2001, pp. 317–320.